JACS
JOURNAL OF THE AMERICAN CHEMICAL SOCIETY
Communication
pubs.acs.org/JACS

Umbellate Distortions of the Uranyl Coordination Environment Result in a Stable and Porous Polycatenated Framework That Can Effectively Remove Cesium from Aqueous Solutions

Yanlong Wang,[†,‡] Zhiyong Liu,[†,‡] Yuxiang Li,[†,‡] Zhuanling Bai,[†,‡] Wei Liu,[†,‡] Yaxing Wang,[†,‡] Xiaomei Xu,[†,‡] Chengliang Xiao,[†,‡] Daopeng Sheng,[†,‡] Juan Diwu,*[,†,‡] Jing Su,*[,§,∥] Zhifang Chai,[†,‡] Thomas E. Albrecht-Schmitt,[⊥] and Shuao Wang*[,†,‡]

[†]School for Radiological and Interdisciplinary Sciences (RAD-X), Soochow University, 199 Ren'ai Road, Suzhou 215123, China

[‡]Collaborative Innovation Center of Radiation Medicine of Jiangsu Higher Education Institutions, 199 Ren'ai Road, Suzhou 215123, China

[§]Shanghai Institute of Applied Physics and Key Laboratory of Nuclear Radiation and Nuclear Energy Technology, Chinese Academy of Sciences, Shanghai 201800, China

[∥]Department of Chemistry & Key Laboratory of Organic Optoelectronics and Molecular Engineering of the Ministry of Education, Tsinghua University, Beijing 100084, China

[⊥]Department of Chemistry and Biochemistry, Florida State University, 95 Chieftain Way, Tallahassee, Florida 32306, United States

Supporting Information

ABSTRACT: Searching for new chemically durable and radiation-resistant absorbent materials for actinides and their fission products generated in the nuclear fuel cycle remain highly desirable, for both waste management and contamination remediation. Here we present a rare case of 3D uranyl organic framework material built through polycatenating of three sets of graphene-like layers, which exhibits significant umbellate distortions in the uranyl equatorial planes studied thoroughly by linear transit calculations. This unique structural arrangement leads to high β and γ radiation-resistance and chemical stability in aqueous solutions within a wide pH range from 3 to 12. Being equipped with the highest surface area among all actinide compounds known to date and completely exchangeable $[(CH_3)_2NH_2]^+$ cations in the structure, this material is able to selectively remove cesium from aqueous solutions while retaining the polycatenated framework structure.

The nuclear waste management especially for actinides and their fission products generated in the nuclear fuel cycle is one of the major challenges and environmental problems of the 21st century. Besides, nuclear weapon testing and plutonium production during the cold war, along with nuclear accidents such as recent catastrophe at the *Fukushima Daiichi* nuclear plant in Japan, have resulted in the contamination of large areas of oceans, groundwater, and sediments by vast amounts of radioisotopes. Current strategies for waste partitioning and contamination remediation (e.g., selective removal of heat-generating cesium and strontium) are facing significant scientific and technological challenges,[1] and their improvement still heavily relies on more sophisticated knowledge of these radioisotopes.

The ability to control the coordination chemistry of actinides is limited when compared to that of main group and transition metal elements and is even more poorly understood than that of lanthanides because the valence orbitals of 5f elements are involved in bonding.[2] Typically, actinides with penta- or hexavalent oxidation states are found within linear actinyl cations $[AnO_2]^{+/2+}$ (An = U, Np, Pu, Am), which forces further coordination in the equatorial plane to be perpendicular to the actinyl unit, affording tetragonal, pentagonal, and hexagonal bipyramidal coordination geometries.[3] If bridging by oxo atoms or other coordinating ligands is not observed,[4] these bipyramids condense to form layered structures. However, there are several exceptions to this situation. First, a series of uranyl clusters have been isolated that form as the result of curvature created by bridging peroxide groups.[5] Second, rare cases exist where steric and electrostatic factors break the linearity of uranyl cations, where much decreased O≡U≡O angles from 180° can be observed.[6] Third, the arrangement of equatorially coordinating atoms could also deviate significantly from ideal planarity resulting in distorted actinyl bipyramidal geometries, but such phenomenon is limited to a handful of sterically congested uranyl complexes combined with N-donor ligands.[7]

We recently started a project focusing on the coordination chemistry of actinides with large conjugated polycarboxylate ligands. This class of ligands has been utilized substantially in building microporous metal−organic framework (MOF) structures.[8] A full investigation on the literature reveals that most of the uranyl(VI) carboxylates reported thus far only utilize simple aliphatic and aromatic carboxylate ligands, where no significant distortion of the corresponding uranyl coordination geometries is observed.[9] In this work, two conjugated polycarboxylate ligands, namely, 1,3,5-tri(4′-carboxylphenyl) benzoic acid (H_3L1) with C_3 symmetry and the desymmetrized

Received: March 9, 2015
Published: May 5, 2015

DOI: 10.1021/jacs.5b02480
J. Am. Chem. Soc. 2015, 137, 6144−6147

version, 3,5-di(4′-carboxylphenyl) benzoic acid (H_3L2), are selected (Figure 1a,b). The solvothermal reaction of H_3L1 with

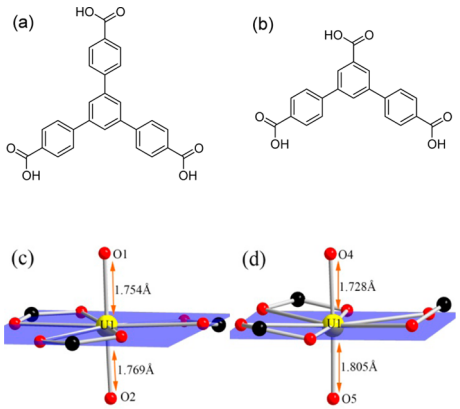

Figure 1. Schematic diagram structures of H_3L1 (a) and H_3L2 (b); coordination environments of $[UO_2]^{2+}$ ions in compounds **1** (c) and **2** (d) with corresponding U≡O bond distances. The light purple planes represent the ideal equatorial configuration perpendicular to the uranyl units.

$UO_2(NO_3)_2{\cdot}6H_2O$ in DMF and nitric acid affords $[(CH_3)_2NH_2][UO_2(L1)]{\cdot}DMF{\cdot}6.5H_2O$ (**1**), whereas $[(CH_3)_2NH_2][UO_2(L2)]{\cdot}0.5DMF{\cdot}15H_2O$ (**2**) is obtained via solvothermal reaction of H_3L2 with $UO_2(NO_3)_2$ in the presence of DMF and water.

Single-crystal X-ray diffraction analysis reveals that compound **1** displays a layered structure and crystallizes in the chiral, trigonal, space group $P3_121$. Circular dichroism (CD) spectrum was adopted to confirm the absolute chiral configuration of **1** (Figure S2). The asymmetric unit of **1** consists of two sets of similar coordination moieties with each one containing one uranyl unit and one L1 ligand. Both uranium ions show almost ideal hexagonal bipyramidal coordination geometries (Figure 1c). The equatorial planes of uranyl units are coordinated by six oxygen atoms from three carboxylate groups. This structural type is well-documented in several uranyl(VI) carboxylates described as open honeycomb-like layered structures.[10] The key feature of **1** is its graphene-like (6,3) net topology displaying nanoscale six-membered ring windows (Figure 2a). The effective size of the window is ca. 15 × 15 Å, which is the largest among the known uranyl layered compounds. $\pi-\pi$ interactions are present between adjacent layers creating stacks with chirality-originating 3_1 symmetry along *c* axis (Figures 2b and S1). The axial U≡O bond distances are all within the normal range from 1.754 (7) Å to 1.776 (6) Å (Table S2).

Reduction of ligand symmetry while maintaining the same coordinating moieties is achieved by replacing L1 with L2. The overall architecture of **2** is substantially different from that of **1**. Compound **2** crystallizes in the noncentrosymmetric hexagonal space group $P\bar{6}2c$. As shown in Figure 1d, the uranium ion in **2** exhibits the same coordination number as found in **1**, where six oxygen atoms from three carboxylate groups bind to one uranyl unit. Notably, unlike **1**, the equatorial plane of the uranyl group reveals significant distortions from an idealized geometry. The O≡U−O bond angles between the uranyl axis and the equatorial plane deviate significantly from 90° and range from 85.3(3) to 89.59(16)° (Table S3). In addition, all six oxygen atoms bend toward the same direction, affording an umbrella-shaped geometry (Figure 1d). The adjacent distorted uranyl units are connected in the opposite direction via L2 ligand,

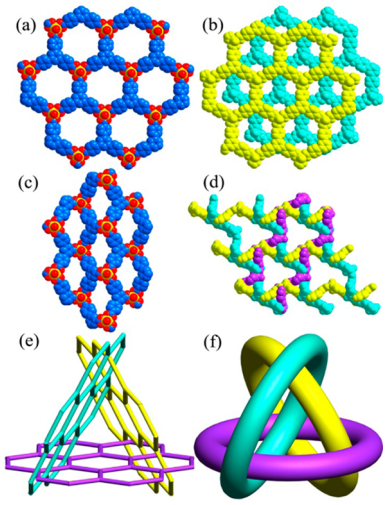

Figure 2. Two-dimensional layered structures of compounds **1** (a) and **2** (c); (b) $\pi-\pi$ stacking in **1**; (d) an overvierw of crystal structure of **2**; (e) topological representation of **2** clearly showing the three-set polycatenation; (f) simplification of polycatenation in **2**. All hydrogen atoms and solvent molecules are omitted for clarity.

generating a series of 2D sinusoidal layers (Figure 2c,d), which can be also simplified as a (6,3) net. The layers in **2** appear compressed when compared to the flat layers in **1** (Figure 2c). Six-membered ring windows are also present in the layer. However, as a result of the distortion, the effective size of the window shrinks to ca. 10 × 10 Å. Two axial U≡O bonds in the distorted uranyl unit are also much more asymmetric compared to **1**, with bond distances of 1.728(8) Å and 1.805(9) Å, respectively. It is surprising that the U≡O4 bond on the same direction of equatorial distortion is 0.077 Å shorter than the other (U≡O5) (Figure 1d). This indicates a substantial change of the uranyl electronic structure initiated by equatorial distortions, similar as the case of bridging uranyl oxo atom with elongated U≡O bond.[4]

More strikingly, three sets (shown in three different colors in Figure 2d−f) of crystallographically equivalent (6,3) wavy nets are entangled together resulting in an extremely rare case of a 2D + 2D → 3D polycatenated framework. Entangled systems as a unique subset of MOFs, including interpenetrating networks, polycatenated networks, polythreading networks, polyknotting networks, etc., are of importance in part for their structural novelty and topological diversity.[11] Polycatenated networks are relatively less common and more special since the dimensionality of overall crystal structure is upgraded when polycatenation is present, while interpenetration does not change the dimensionality. This contrasts sharply with the situation in **1** where $\pi-\pi$ stacking is facilitated by the flat layers, while the wavy layer configuration in **2** originating from the distorted U(VI) environment inhibits the corresponding $\pi-\pi$ stacking, generating the first example of an f-element polycatenated framework. The free void volume of **2** is 48.9%, and large triangle-shaped channels are observed in three different directions (Figure 2d). $[(CH_3)_2NH_2]^+$ cations can be found on the electron density map in low symmetry structural solutions but are highly disordered, indicating its ion-exchange ability at the first place.

To understand the influence of the equatorial distortion on the interaction between uranyl and polycarboxylate ligands in **2**, linear transit (LT) calculations were performed on two model compounds $[UO_2(RCOO)_3]^-$ (R = H, Ph) along $\angle O_{t1}UO_c$

DOI: 10.1021/jacs.5b02480
J. Am. Chem. Soc. 2015, 137, 6144−6147

decreasing direction, where O_t is the axial uranyl oxo atom and O_c means equatorial oxo atom.[12] As these two compounds give almost the same trend of bond lengths between uranium and coordinated oxygen atoms, we only take $[UO_2(HCOO)_3]^-$ as an example to illustrate, while presenting the calculation results of $[UO_2(PhCOO)_3]^-$ in Figure S5. When $\angle O_{t1}UO_c$ decreases from 90° to 70°, the U≡O_{t1} bond length decreases by 0.04 Å, and the U≡O_{t2} bond length varies little with a slight increase of 0.01 Å (Figure 3). The opposite trends of R(U≡O_{t1}) and R(U≡O_{t2})

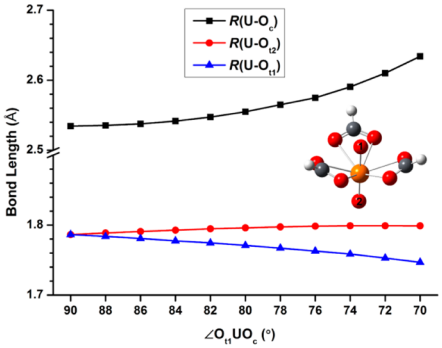

Figure 3. Trend of bond lengths between uranium and coordinated oxygen atoms in $[UO_2(HCOO)_3]^-$ as the decrease of $\angle O_{t1}UO_c$: R(U≡O_{t1}), R(U≡O_{t2}), and R(U−O_c), where O_t means terminal oxygen of uranyl unit and O_c means carboxyl oxygen.

are due to the difference in the ligand field repulsion imposed on the two terminal oxygen atoms. The key message here is that the strong repulsion from umbrella-shaped $HCOO^-$ ligands pushes O_{t1}'s valence orbitals up to a higher energy level, producing a better energy matching with uranium's valence orbitals and enhancing the U≡O_{t1} bonding. Simultaneously, the U≡O_{t2} bonding is weakened due to an increasing mismatch in energy level arising from the reduced ligand repulsion. It should be noted that the experimental value of the bond distance difference between R(U≡O_{t1}) and R(U≡O_{t2}) (0.077 Å) is larger than the calculation value (~0.02 Å) and that using a larger ligand $PhCOO^-$ to replace $HCOO^-$ does not improve this agreement, which is most likely due to the effects from the compact three-set polycatenation structure, and more specifically the strong interactions between polycatenated layers marked in different colors in Figure 2d, which give rise to strong ligand fields imposing on one of the two terminal oxygen atoms, i.e., O_4 in Figure 1d. The distances between the terminal O_4 atom and the three nearest ligand hydrogen atoms in the polycatenated layer are 2.47, 2.47, and 2.97 Å, respectively, in compound **2**, shown in Figure S6.

Figure 4 qualitatively illustrates the influence of the equatorial distortion on the valence orbital energy levels of uranyl and its constitutive O atoms, on the molecular orbital compositions and shapes, and on the U≡O_t bond lengths by the comparison between equatorial ligand fields of $D_{\infty h}$ and $C_{\infty v}$ symmetry, respectively. The pushed-up O_{t1} 2p shell interacts with U 5f better than U 6d orbitals and mainly contributes to the upper U≡O bonding orbitals (2σ and 2π), while O_{t2} 2p better overlaps with U 6d and contributes more to the lower ones (1σ and 1π). This is because relatively contracted U 5f orbitals have a good radial match with closer O_{t1} 2p shell, and more diffuse U 6d orbitals match well with distant O_{t2} 2p shell. Besides, the R(U−O_c) increases by 0.10 Å as the $\angle O_{t1}UO_c$ decreases, owing to the weakened interaction between uranyl and $RCOO^-$ (R = H, Ph) ligands (Figures S7, S8 and Tables S4, S5). Clearly, the equatorial

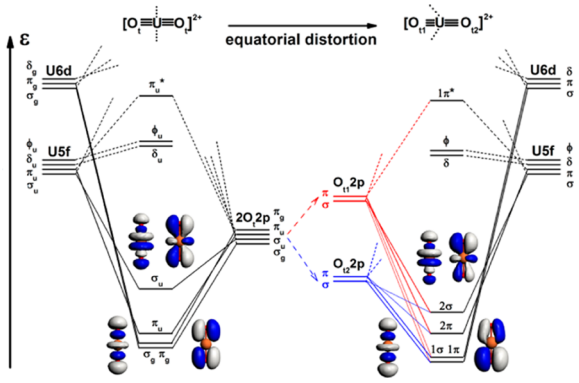

Figure 4. Valence-orbital energy levels of $[OUO]^{2+}$ and of its constitutive atoms in an undistorted ($D_{\infty h}$ symmetry) and umbrella-distorted ($C_{\infty v}$ symmetry) equatorial ligand field, respectively, represented by dotted lines on top of and down below U atom, and illustration of the equatorial distortion influence on the orbital energy levels, orbital compositions and shapes, and U≡O bond lengths. The O_{t1} 2p mainly contributes to U≡O 2σ and 2π orbitals connected by a thicker solid line in red, and O_{t2} 2p to 1σ and 1π orbitals connected by a thicker solid line in blue.

distortion of the ligand coordination (i.e., steric repulsion between ligand and uranyl) can be used to adjust the axial uranium−oxygen bonding.

In addition, when $\angle O_{t1}UO_c$ decreases, both of the steric and orbital interactions become relatively positive, as well as the resulting total bonding energy. This bonding analysis result shows that both ionic and covalent interaction between uranyl and $RCOO^-$ (R = H, Ph) ligands are weakened as the ligand coordination gradually departs from the equatorial plane. The resulting energetic instability is not significant, which is estimated to be less than 16 kJ/mol in energy when $\angle O_tUO_c$ is higher than 84°. This small energy change will not strongly affect the stability of the crystal structure, confirmed by the following stability measurements. The interactions of orbitals in a_2 and e symmetry are weakened as the orbital overlap of O_c 2p valence shell with U 5fϕ and 6dδ orbitals is greatly reduced in equatorial plane. The comparisons of the corresponding orbital envelopes between the geometrical structures with $\angle O_tUO_c$ of 90° and 70° for $[UO_2(HCOO)_3]^-$ are shown in Table S6.

Compound **2** exhibits permanent porosity confirmed by the reversible N_2 adsorption and desorption isotherm at 77 K (Figure S11). Moreover, compound **2** uptakes as high as 274 cm^3 g^{-1} N_2 with a BET surface area of 924 cm^2 g^{-1} (Langmuir: 1068 cm^2 g^{-1}), which is the highest among all measured actinide compounds up to date.[13] However, the high surface area of **2** does not sacrifice its stability as it is highly stable and can well maintain its crystallinity in aqueous solutions within a wide pH range from 3 to 12 (Figure S12). In addition, we observe no structural and crystal degradation for both compounds **1** and **2** even under 200 kGy ^{60}Co γ irradiation with the dose rate of 1.2 kGy/hour (Figures S13 and S14) and 200 kGy β irradiation (1.2 MeV) provided by an electron accelerator with the dose rate of 20 kGy/hour (Figure S15 and S16), respectively, indicating excellent radiation resistances of these two phases.

Being equipped with open channels that pierce the whole structure and crystallographically disordered $[(CH_3)_2NH_2]^+$ cations in the channels, compound **2** is well suited for ion exchange studies, especially for cesium ion as a highly radioactive and heat-generating fission product. Notably, By soaking crystals of **2** in an aqueous solution with a moderate Cs^+ concentration

DOI: 10.1021/jacs.5b02480
J. Am. Chem. Soc. 2015, 137, 6144−6147

(500 ppm), nearly 100% of $[(CH_3)_2NH_2]^+$ originally present in the structure can be rapidly substituted with Cs^+, demonstrated from the atomic ratio of Cs/U ≈ 1 in the Cs^+ exchanged crystals (Figure S17), indicating a high exchange capacity toward cesium possessed by **2**. Additionally, the polycatenated framework structure was completely retained during the ion exchange process indicated by powder X-ray diffraction data (Figure S18). A full cesium exchange investigation was then conducted, and the selected results are shown in Tables S7−S10. The cesium capture ability of **2** characterized by distribution coefficient K_d is at the same order of commercial functional materials as well as several synthetic cesium absorbents reported recently although the molar amount of exchangeable cations per unit of absorbent mass is not as large as other materials (molecular weight of **2** is relatively large).[14] Compound **2** was able to remove up to 94.51% of Cs^+ from solutions and the absorption equilibrium can be reached within 20 minutes (Figure S19). More importantly, with the addition of 5 or 20 mass equivalences of exchange-competing Li^+, Na^+, K^+, Rb^+, Mg^{2+}, or Ca^{2+} cations to the initial 1 ppm of Cs^+ solutions, no significant decrease of Cs^+ removal was observed, and the removing percentage ranging from 71.81% to 93.50% can be still achieved, indicating a good exchange selectivity toward Cs^+ owned by **2** (Table S8).

In conclusion, by reducing the symmetry of coordinating ligands with the same donor atoms, we observed a substantial structural transformation from a 2D graphene-like layered structure to an unusual case of three-set polycatenated 3D framework. This transformation is accompanied by a significant umbellate distortion of the uranyl equatorial plane and concomitant subtle energetic instability shown by LT calculations. The unique structural arrangement leads to high radiation-resistance and chemical stability in aqueous solutions. Compound **2** is able to selectively remove cesium from aqueous solutions while retaining the framework structure, providing a potentially useful material for dealing with mobile fission products during waste partitioning and contamination remediation processes.

■ ASSOCIATED CONTENT

Supporting Information

Synthesis methods, X-ray crystallography, CD, SHG, PXRD, spectroscopic characterizations, TGA, BET, Cs^+ exchange, and computational details. The Supporting Information is available free of charge on the ACS Publications website at DOI: 10.1021/jacs.5b02480.

■ AUTHOR INFORMATION

Corresponding Authors

*shuaowang@suda.edu.cn.
*diwujuan@suda.edu.cn.
*sujing@sinap.ac.cn.

Notes

The authors declare no competing financial interest.

■ ACKNOWLEDGMENTS

This work was supported by grants from the National Science Foundation of China (91326112, 21422704, 21471107, 21201106, 41303006), the Science Foundation of Jiangsu Province (BK20140007), a Project Funded by the Priority Academic Program Development of Jiangsu Higher Education Institutions (PAPD) and Jiangsu Provincial Key Laboratory of Radiation Medicine and Protection, "Young Thousand Talented Program" in China, "Strategic Priority Research Program" of the Chinese Academy of Sciences (Grant No. XDA02040104), and the Program of International S&T Cooperation (2014DFG60230, ANSTO-SINAP).

■ REFERENCES

(1) (a) Ewing, R. C. *Proc. Natl. Acad. Sci. U.S.A.* **1999**, *96*, 3432−3439. (b) Grambow, B. *Elements* **2006**, *2*, 357−364. (c) Lumpkin, G. R. *Element* **2006**, *2*, 365−372. (d) Bortun, A. I.; Bortun, L. N.; Poojary, D. M.; Xiang, O.; Clearfield, A. *Chem. Mater.* **2000**, *12*, 294−305.

(2) (a) Neidig, M. L.; Clark, D. L.; Martin, R. L. *Coord. Chem. Rev.* **2013**, *257*, 394−406. (b) Polinski, M. J.; Garner, E. B.; Maurice, R.; Planas, N.; Stritzinger, J. T.; Parker, T. G.; Cross, J. N.; Green, T. D.; Alekseev, E. V.; Van Cleve, S. M.; Depmeier, W.; Gagliardi, L.; Shatruk, M.; Knappenberger, K. L.; Liu, G.; Skanthakumar, S.; Soderholm, L.; Dixon, D. A.; Albrecht-Schmitt, T. E. *Nat. Chem.* **2014**, *6*, 387−392.

(3) (a) Burns, P. C. *Can. Mineral.* **2005**, *43*, 1839−1894. (b) Natrajan, L. S. *Coord. Chem. Rev.* **2012**, *256*, 1583−1603.

(4) (a) Volkringer, C.; Henry, N.; Grandjean, S.; Loiseau, T. *J. Am. Chem. Soc.* **2012**, *134*, 1275−1283. (b) Sullens, T. A.; Jensen, R. A.; Shvareva, T. Y.; Albrecht-Schmitt, T. E. *J. Am. Chem. Soc.* **2004**, *126*, 2676−2677. (c) Alekseev, E. V.; Krivovichev, S. V.; Depmeier, W.; Siidra, O. I.; Knorr, K.; Suleimanov, E. V.; Chuprunov, E. V. *Angew. Chem., Int. Ed.* **2006**, *45*, 7233−7235.

(5) (a) Qiu, J.; Burns, P. C. *Chem. Rev.* **2013**, *113*, 1097−1120. (b) Sigmon, G. E.; Unruh, D. K.; Ling, J.; Weaver, B.; Ward, M.; Pressprich, L.; Simonetti, A.; Burns, P. C. *Angew. Chem., Int. Edit* **2009**, *48*, 2737−2740. (c) Qiu, J.; Ling, J.; Jouffert, L.; Thomas, R.; Szymanowski, J. E. S.; Burns, P. C. *Chem. Sci.* **2014**, *5*, 303−310.

(6) (a) Wu, S.; Kowalski, P. M.; Yu, N.; Malcherek, T.; Depmeier, W.; Bosbach, D.; Wang, S.; Suleimanov, E. V.; Albrecht-Schmitt, T. E.; Alekseev, E. V. *Inorg. Chem.* **2014**, *53*, 7650−7660. (b) Szigethy, G.; Raymond, K. N. *J. Am. Chem. Soc.* **2011**, *133*, 7942−7956. (c) Arnold, P. L.; Patel, D.; Wilson, C.; Love, J. B. *Nature* **2008**, *451*, 315−317.

(7) (a) Sessler, J. L.; Seidel, D.; Vivian, A. E.; Lynch, V.; Scott, B. L.; Keogh, D. W. *Angew. Chem., Int. Ed.* **2001**, *40*, 591−594. (b) Berthet, J.-C.; Thuéry, P.; Dognon, J.-P.; Guillaneux, D.; Ephritikhine, M. *Inorg. Chem.* **2008**, *47*, 6850−6862. (c) Copping, R.; Jeon, B.; Pemmaraju, C. D.; Wang, S.; Teat, S. J.; Janousch, M.; Tyliszczak, T.; Canning, A.; Groenbech-Jensen, N.; Prendergast, D.; Shuh, D. K. *Inorg. Chem.* **2014**, *53*, 2506−2515.

(8) (a) Li, J.-R.; Sculley, J.; Zhou, H.-C. *Chem. Rev.* **2012**, *112*, 869−932. (b) Chae, H. K.; Siberio-Perez, D. Y.; Kim, J.; Go, Y.; Eddaoudi, M.; Matzger, A. J.; O'Keeffe, M.; Yaghi, O. M. *Nature* **2004**, *427*, 523−527. (c) O'Keeffe, M.; Yaghi, O. M. *Chem. Rev.* **2012**, *112*, 675−702.

(9) (a) Andrews, M. B.; Cahill, C. L. *Chem. Rev.* **2013**, *113*, 1121−1136. (b) Wang, K.-X.; Chen, J.-S. *Acc. Chem. Res.* **2011**, *44*, 531−540.

(10) Go, Y. B.; Wang, X. Q.; Jacobson, A. J. *Inorg. Chem.* **2007**, *46*, 6594−6600.

(11) Carlucci, L.; Ciani, G.; Proserpio, D. M. *Coord. Chem. Rev.* **2003**, *246*, 247−289.

(12) Theoretical calculations were performed using density functional theory at the B3LYP level. The computational details are described in the Supporting Information.

(13) (a) Ok, K. M.; Sung, J. Y.; Hu, G.; Jacobs, R. M. J.; O'Hare, D. *J. Am. Chem. Soc.* **2008**, *130*, 3762−3763. (b) Alsobrook, A. N.; Hauser, B. G.; Hupp, J. T.; Alekseev, E. V.; Depmeier, W.; Albrecht-Schmitt, T. E. *Chem. Commun.* **2010**, *46*, 9167−9169. (c) Falaise, C.; Charles, J.-S.; Volkringer, C.; Loiseau, T. *Inorg. Chem.* **2015**, *54*, 2235−2242.

(14) (a) Ding, N.; Kanatzidis, M. G. *Nat. Chem.* **2010**, *2*, 687−691. (b) Feng, M. L.; Kong, D. N.; Xie, Z. L.; Huang, X. Y. *Angew. Chem., Int. Ed.* **2008**, *120*, 8751−8754. (c) Datta, S. J.; Moon, W. K.; Choi, D. Y.; Hwang, I. C.; Yoon, K. B. *Angew. Chem., Int. Ed.* **2014**, *53*, 1−7. (d) Manos, M. J.; Kanatzidis, M. G. *J. Am. Chem. Soc.* **2009**, *131*, 6599−6607.

DOI: 10.1021/jacs.5b02480
J. Am. Chem. Soc. 2015, 137, 6144−6147